In situ Characterization of Mesoporous Co/CeO_2 Catalysts for the High Temperature Water-Gas Shift

Dimitriy Vovchok [a, b], *Curtis J. Guild* [c], *Shanka Dissanayake* [c], *Jordi Llorca* [d], *Eli Stavitski* [e], *Zongyuan Liu* [b], *José A. Rodriguez* [a, b], *Steven L. Suib,* [a, c, *] *Sanjaya D. Senanayake* [b, *]

[a] Department of Chemistry, Stony Brook University, Stony Brook, NY, 11794

[b] Chemistry Department, Brookhaven National Laboratory, Upton, NY, 11973

[c] Department of Chemistry, University of Connecticut, 55 N. Eagleville Rd., Storrs, CT 06269

[d] Institute of Energy Technologies, Department of Chemical Engineering and Barcelona Research Center in Multiscale Science and Engineering. Technical University of Catalonia. Barcelona 08019, Spain

[e] National Synchrotron Light Source II. Brookhaven National Laboratory, Upton, NY, 11973

[*] Corresponding author: Bldg. 555A, Brookhaven National Lab, P.O. Box 5000, Upton, NY 11973-5000, 631-344-4343, Steven.suib@uconn.edu ; ssenanay@bnl.gov

Abstract

Mesoporous Co/CeO_2 catalysts were found to exhibit significant activity for the high temperature water-gas shift (WGS) reaction with cobalt loadings as low as 1%. The catalysts feature a uniform dispersion of cobalt within the CeO_2 fluorite type lattice with no evidence of discrete cobalt phase segregation. Operando XANES and ambient pressure XPS experiments were used to elucidate the active state of the catalysts as partially reduced cerium oxide doped with oxidized cobalt atoms. Operando XRD and DRIFTS experiments suggest facile cerium reduction and oxygen vacancy formation, particularly with lower cobalt loadings. Operando DRIFTS analysis also revealed the presence of surface carbonate and bidentate formate species under reaction conditions, which may be associated with additional mechanistic pathways for the WGS reaction. Deactivation behavior was observed with higher cobalt loadings. XANES data suggests the formation of small metallic cobalt clusters at temperatures above 400°C may be responsible. Notably, this deactivation was not observed for the 1% cobalt loaded catalyst, which exhibited the highest activity per unit cobalt.

Introduction

Production of pure hydrogen gas for renewable fuel and chemical synthesis applications remains an area of significant research interest. Currently, over 95% of the world's hydrogen supply is produced through the reforming of fossil fuels[1]. This reforming process necessarily generates a product stream (reformate gas or syngas[2]) with a significant concentration of carbon monoxide. The CO content is highly detrimental to the application of hydrogen towards synthesis processes and hydrogen fuel cells, since CO acts as a catalyst poisoning agent[3]. For this reason, the removal of CO from reformate gas feeds is necessitated as a part of the hydrogen generation process.

The water-gas shift (WGS: $CO + H_2O \rightarrow CO_2 + H_2$, $\Delta H = -41$ kJ mol^{-1}) reaction[4] is widely applied to industrial hydrogen generation processes in order to remove CO from reformate gas, and generate additional hydrogen product[5]. The WGS is typically carried out with the help of heterogeneous catalyst materials in two temperature stages in order to take advantage of both kinetic and thermodynamic properties of the mildly exothermic reaction[6-7]. The high temperature stage (HT-WGS) is typically carried out at between 350-450°C, although in some cases this temperature can be as high as 600°C[8-9]. Ferrochrome[10] and other iron based catalysts[11-12] are commonly used for the HT-WGS reaction.

Well-dispersed metals supported on cerium oxide have been frequently studied as catalysts for both low temperature and high temperature water gas shift reactions[13-15]. Cerium oxide is often considered an active catalytic support material due to its excellent reducibility and oxygen transport properties[16-18] and strong metal-support interactions[19]. Oxygen vacancy sites

present in partially reduced ($Ce^{4+} \rightarrow Ce^{3+}$) cerium oxide have been identified as playing a role in the dissociation of water during the WGS reaction[20-21], while supported metal particles account for the adsorption and activation of the CO molecule. Additionally, an associative WGS reaction pathway is available on the surface of these materials through the formation of H_xCO_y intermediate species such as formates, carbonates, and carboxyls[22].

In recent years, a novel sol-gel synthesis technique was developed to produce a highly crystalline, monodisperse, and mesoporous CeO_2 morphology[23]. The resulting material demonstrated significant activity for the WGS reaction as a standalone, metal free catalyst[24]. In a subsequent study, we have successfully synthesized and evaluated the activity and unique metal-support interactions of copper loaded mesoporous CeO_2 catalysts for the low temperature WGS reaction[25]. Building upon this work, we have synthesized mesoporous Co/CeO_2 materials with Co loadings between 1% and 10% as potential catalysts for the high temperature WGS reaction. Relatively high loading (15%-35%) Co/CeO_2 catalysts have been reported as active for the HT-WGS in recent studies[26-27], with activity being attributed to strong metal-support interactions enhancing a segregated Co_3O_4 phase, which is known to have significant CO oxidation capabilities[28]. In this study, we examine mesoporous Co/CeO_2 materials that do not exhibit an observable segregated cobalt oxide phase, and demonstrate significant catalytic activity for the HT-WGS reaction with low loadings of cobalt. For the purposes of this study, the 1%, 5%, and 10% mesoporous Co/CeO_2 materials will be abbreviated as **1CoCe**, **5CoCe**, and **10CoCe**, respectively.

Experimental

Catalyst Synthesis

Mesoporous cobalt doped CeO_2 catalysts were synthesized using the sol-gel synthesis method[23]. For the synthesis of 1% Co/CeO_2 catalysts, 8.7g of $Ce(NO_3)_3 \cdot 6H_2O$, 0.059 g of $Co(NO_3)_2 \cdot 6H_2O$, 3g of Pluronic-P-123, and 1.5 mL nitric acid were mixed in 1.5 mL 1-Butanol at 60 °C to form a homogeneous solution. The solution was heated in a ventilated oven at 120 °C for about 2.5 hours. The products were cooled, washed in excess ethanol, and dried under vacuum overnight. The solids were then loaded into alumina crucibles and heated to the calcination temperature of 450°C with a ramp rate of 5 °C/min. The samples were kept at 450°C for 4 hours. Higher cobalt loadings (5% and 10%) were prepared using the same procedure except with 5% and 10% molar ratios of cobalt to cerium.

Transmission Electron Microscopy

High resolution transmission electron microscopy (HRTEM) and scanning transmission electron microscopy (STEM-HAADF-EDX) characterization was carried out at the Technical University of Catalonia using a Tecnai G2 F20 S-TWIN microscope equipped with a field emission electron source and operated at 200 kV. Samples were dispersed in alcohol suspension and supported on holey carbon film over the grid.

Textural Studies

N_2 sorption experiments on the mesoporous ceria were performed with a Quantachrome Autosorb-1−1C automated sorption system. All the samples were degassed at 150°C for 6 hours under vacuum prior to measurement. The surface areas were calculated using the Brunauer−Emmett−Teller (BET) method, and pore sizes and volumes were calculated from the desorption branch of the isotherm using the Barrett−Joyner−Halenda (BJH) method.

Catalytic Activity studies

The catalytic activity was evaluated in a home-built horizontal fixed-bed reactor equipped with a gas manifold and a standardized process gas chromatograph (GC, SRI International Multi-gas #2) for sampling the outlet gas. About 50 mg of catalyst were packed into a quartz reactor and supported by quartz wool. The catalyst was cleaned under flowing helium at 200°C for an hour, cooled to room temperature, and then was exposed to the WGS conditions (5% CO, 3% H_2O, balance He). The catalyst was then ramped to 300^{o}C and temperatures taken in 50 degree increments up to 500^{o}C. At each temperature, 3 data points were taken.

X-ray Photoelectron Spectroscopy (XPS)

Ambient pressure XPS measurements were carried out at Brookhaven National Laboratory (BNL). Powder sample was pressed into an aluminum plate, and introduced into ultra-high vacuum environment, where a conventional Mg X-ray source was used to probe the material. Ambient pressure measurements were collected after introducing 25 mTorr CO and 25 mTorr H_2O into the chamber and heating the sample stepwise to 100, 200, and 400^{o}C. The Ce 3d region was plotted and analyzed using CasaXPS software[29].

Operando Synchrotron X-ray Diffraction (XRD)

Operando X-ray Diffraction (XRD) experiments detailed in this study were performed at Advanced Photon Source (APS) in Argonne National Laboratory at beamline 17BM-B. The experiments were carried out using the Clausen[30] capillary flow reactor. A quartz capillary with an inner diameter of 0.9mm and outer diameter of 1.1mm was loaded with approximately 5mg of sample between two segments of quartz wool. Reactant gas consists of 5% CO (in Helium) flown through a room temperature water bubbler to achieve 3% H_2O concentration. The reactant

gas mixture is flown continuously through the capillary at a rate of 10 cc/min. The temperature of the reactor cell is controlled using a controlled resistance heating coil. The temperature profile for the experiments consisted of stepwise heating and cooling up to 400°C. X-ray Diffraction patterns are collected continuously during the experiment. Outflow gas during XRD experiments was analyzing using a Residue Gas Analyzer (RGA) quadrupole mass spectrometry unit in order to provide a qualitative WGS activity analysis by monitoring the production of H_2 and CO_2 gas. The X-ray wavelength utilized for XRD was either 0.72768 Å or 0.45336 Å, depending on sample, since the data sets were collected over the course of several scheduling intervals with different beamline configurations. X-ray Diffraction patterns were plotted in Origin and processed using the GSAS II software[31] to obtain structural information via Rietveld refinement[32].

X-ray Absorption Spectroscopy (XAS)

Operando Co K-edge X-ray Absorption Near-Edge Structure (XANES) measurements were carried out under WGS reaction environment conditions (5% CO, 3% H_2O, balance He) at beamline 8-ID (ISS) at the National Synchrotron Light Source II (NSLS-II) at Brookhaven National Laboratory, which is a high flux (10^{14} at 10keV) wiggler spectroscopy beamline equipped with a Si 111 double crystal high heat load monochromator. An identical reaction cell environment was used as described for X-ray diffraction experiments. The reaction cell was heated stepwise and XANES measurements were collected at 20, 100, 200, 300, 400 and 500°C using an array of silicon drift fluorescence detectors.

Ex-situ Co K-edge extended edge X-ray absorption fine structure (EXAFS) measurements were also carried out at beamlines 8-ID (ISS) at NSLS-II and 20-ID at APS in fluorescence detection mode. Near-edge X-ray absorption fine structure (NEXAFS) spectra (Co $L_{2,3}$-edge and Ce $M_{4,5}$-

edge) were collected in total electron yield (TEY) mode at beamline 23-ID-2 (CSX-2) at NSLS II. All X-ray absorption data were processed using the Athena software[33]. For the purposes of this study, the term XANES is used to refer to hard X-ray experiments and the equivalent term NEXAFS is used to refer to soft X-ray experiments.

Diffuse Reflectance Infrared Fourier Transform Spectroscopy (DRIFTS)

DRIFTS experiments were performed at the Advanced Energy Center (AERTC) at Stony Brook University. The reactor cell was loaded with sample material and heated to 100°C, followed by stepwise heating in 100°C increments up to 500 °C under WGS reaction environment conditions (5% CO, 3% H_2O, balance He). Infrared spectra (4000 to 600 cm^{-1}) were recorded every 85 seconds. KBr background was subtracted from all spectra. Data were processed using Thermo Scientific OMNIC 8 software.

Results and Discussion

Morphology and Texture

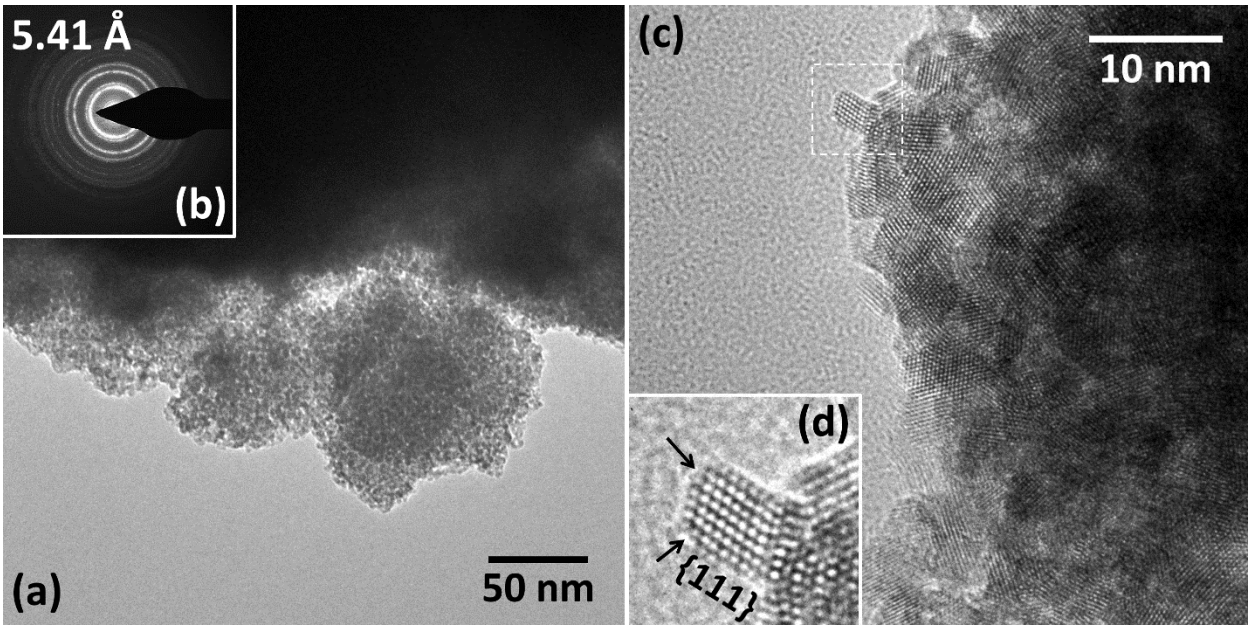

*Figure 1: Imaging of **10CoCe** sample: (a) Low magnification TEM, (b), selected area electron diffraction, (c) high resolution TEM, and (d) single particle inset.*

A transmission electron microscopy study was carried out to examine the local morphology of mesoporous Co/CeO_2 samples with cobalt loadings of 1% (**1CoCe**), 5% (**5CoCe**), and 10% (**10CoCe**). Representative images of **10CoCe** are reported in Figure 1.

The **10CoCe** material was found to consist of highly crystalline, monodisperse nanoparticles measuring 4.0 ± 0.5 nm in diameter. A selected area electron diffraction (SAED) pattern recorded over hundreds of particles indicates a single face centered cubic (fcc) crystalline phase with a lattice parameter of 5.41 Å, consistent with the CeO_2 fluorite lattice[34] (Figure 1b). Close examination of individual crystallites (Figure 1d) reveals a truncated octahedral morphology that almost exclusively exposes {111} crystallographic planes. A 'zig-zag' nanostructure resulting from the removal of several atomic rows is present where {100} planes would be expected (black arrows, Figure 1d). The morphology of these crystallites resembles bare mesoporous CeO_2 materials[24].

No segregated cobalt content was observed for any mesoporous Co/CeO_2 samples. No crystalline cobalt phases (Co, CoO, Co_2O_3, or Co_3O_4) were indicated on SAED patterns. Likewise, no amorphous content was observed in TEM. However, energy-dispersive X-ray spectroscopy (EDX) measurements indicate the presence of Co in constant proportion with Ce, with a concentration of approximately 9.4% for the **10CoCe** sample (Figure S1). These observations suggest a uniform dispersion of cobalt consistent with a solid solution of cobalt within the CeO_2 fluorite lattice.

TEM imaging of **1CoCe** and **5CoCe** (Figure S2) reveals morphology indistinguishable from the **10CoCe** sample. Particle size analysis and lattice parameters as measured by SAED are indistinguishable from those measured for **10CoCe**.

TEM measurements were also collected for a spent (post-mortem) **10CoCe** sample that has been exposed to water-gas shift (WGS) conditions (5% CO, 3% H_2O, balance He) for 24 hours at 400°C (Figure S3). Following exposure to reaction conditions, particle dispersion and Co to Ce ration remained homogenous throughout the sample. The mean particle size increased slightly to 5 ± 1 nm. Crystallites retained their crystallinity, however the 'zig-zag' nanostructure was no longer observed. It is therefore likely that facets other than {111} were exposed under reaction conditions.

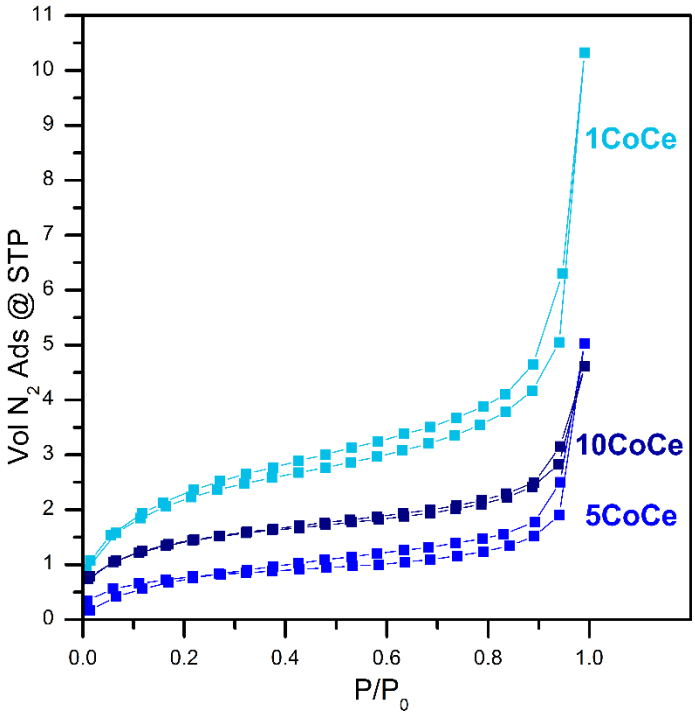

Figure 2: Adsorption isotherms for mesoporous Co/CeO_2 catalysts

Table 1: Textural and particle size properties of mesoporous Co/CeO_2 catalysts.

	Surface area (m^2 g^{-1})	**Pore volume (cc g^{-1})**	**Avg. particle size TEM (nm)**
meso. CeO2	163	0.137	3.5
1CoCe	37	0.072	4.0

5CoCe	23	0.065	4.0
10CoCe	34	0.048	4.0

Nitrogen adsorption isotherms were measured for mesoporous CeO2 and mesoporous Co/CeO_2 materials (Figure 2). The surface area according to Brunauer–Emmett–Teller (BET) theory[35] is reported alongside porosity and particle size in Table 1.

The surface areas of mesoporous Co/CeO_2 materials were measured to be significantly smaller than that of bare mesoporous CeO_2, but were not observed to vary significantly between different cobalt loadings. Likewise, the pore volume was measured to be smaller than that of mesoporous CeO_2, with a slight decreasing trend with increasing cobalt loading. The average particle size for all cobalt containing samples was the same, and slightly larger than mesoporous CeO_2.

Spectroscopic Characterization

The electronic and chemical properties of fresh mesoporous Co/CeO_2 catalysts were probed using a combination of near edge X-ray absorption fine structure (NEXAFS) and X-ray photoelectron spectroscopy (XPS) measurements. Cobalt $L_{2,3}$-edge NEXAFS spectra (Figure 3a) suggest the presence an oxidized cobalt species in all catalysts. The spectra do not indicate a segregated CoO, Co_2O_3, or Co_3O_4 phase, however. The lack of a key lower energy feature at 777.8 eV indicates the absence of octahedrally coordinated Co^{2+} present in CoO[36-37]. The most intense feature at 780.3 eV may be indicative of octahedrally coordinated Co^{3+} ions[38]. No significant variation was noted between the three cobalt loadings. Additionally, the Co $L_{2,3}$-edge

NEXAFS spectra of fresh and spent **10CoCe** samples appear nearly identical, suggesting the chemical state of the cobalt content is recoverable post reaction.

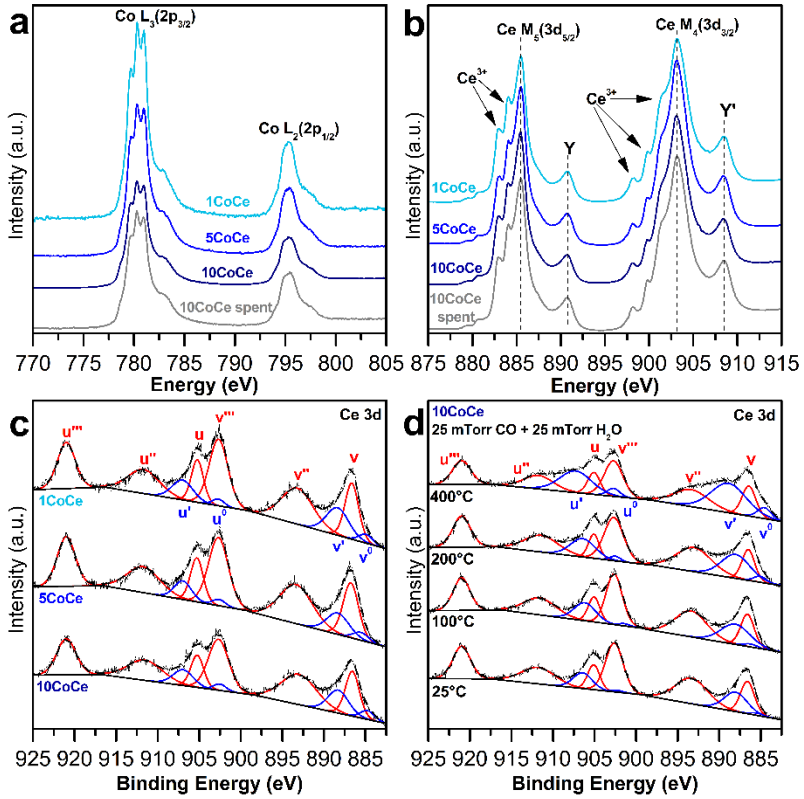

*Figure 3: Spectroscopic study of mesoporous Co/CeO_2 materials: (a) Co $L_{2,3}$ NEXAFS, (b) Ce $M_{4,5}$ NEXAFS, (c) Ce 3d XPS under vacuum conditions and (d) Ce 3d XPS of **10CoCe** under WGS ambient conditions.*

Cerium $M_{4,5}$-edge NEXAFS spectra (Figure 3b) indicate a partially reduced cerium oxide containing both Ce^{3+} and Ce^{4+} ions[39]. No significant differences in the Ce $M_{4,5}$-edge NEXAFS were observed between the three cobalt loadings. The cerium edges of fresh and spent **10CoCe** samples look nearly identical, further demonstrating the recoverable nature of the material.

Cerium $3d_{3/2,5/2}$ XPS spectra for the three mesoporous Co/CeO_2 catalysts are reported in Figure 3c. Ten peaks were fit to each spectrum and labeled according to Burroughs formalism. Each spectrum is composed of five spin-orbit split doublets (**u:** $3d_{3/2}$, **v:** $3d_{5/2}$) split by approximated 18.6 eV. For fitting purposes, the intensity ratio **I**($3d_{5/2}$)/**I**($3d_{3/2}$) was fixed to 1.5 for each doublet pair[40-41]. All Ce $3d_{3/2,5/2}$ XPS spectra measured suggest a partially reduced CeO_2 material with the majority of cerium species in the Ce^{4+} oxidation state. An approximation of the degree of Ce^{4+} to Ce^{3+} reduction was obtained by calculating the percent composition of Ce^{3+} species using Eq. 1.

$$\%Ce^{3+} = \frac{A(u')+A(u0)}{A(u)+A(u')+A(u'')+A(u''')+A(u0)} \quad (1)$$

The Ce^{3+} content as a percentage of total cerium content was calculated to be 19%, 15%, and 18% for **1CoCe**, **5CoCe**, and **10CoCe**, respectively. There are limitations of this calculation, which typically include a significant overestimation of Ce^{3+} content due to issues associated with X-ray irradiation, sample heating due to X-ray exposure, background fitting, and other quantification difficulties[42-43]. Additionally, since XPS is a surface sensitive probe, these concentrations may not reflect bulk Ce^{3+} composition. Given these limitations, the cerium content in all three mesoporous Co/CeO_2 catalysts is partially reduced on the surface without substantial difference with respect to cobalt loading.

Ambient pressure Ce $3d_{3/2,5/2}$ XPS measurements were conducted on the **10CoCe** sample in the presence of 25 mTorr CO and 25 mTorr H_2O to simulate water-gas shift reaction conditions (Figure 3d). The spectra at all temperature steps were fit and labeled as described previously, and Eq. 1 was used to approximate Ce^{3+} concentration. Figure 4 reports the change of Ce^{3+} concentration with temperature under ambient pressure WGS conditions. Heating of the

sample under these conditions resulted in an increase of Ce^{3+} composition from ~20% at room temperature to ~40% at 400°C. This evident reduction of cerium in the CeO_2 lattice facilitates favorable catalytic properties due to the formation of additional oxygen vacancy sites that may serve as H_2O binding and splitting sites during the WGS reaction[20].

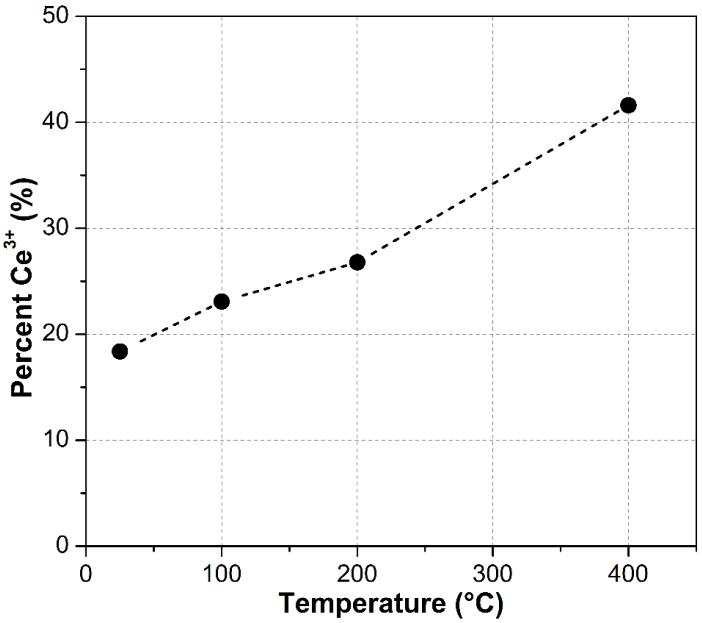

Figure 4: Ce^{3+} concentration as percentage of total cerium content in **10CoCe** calculated from XPS upon heating under ambient pressure WGS conditions.

Water-gas Shift Catalytic Activity

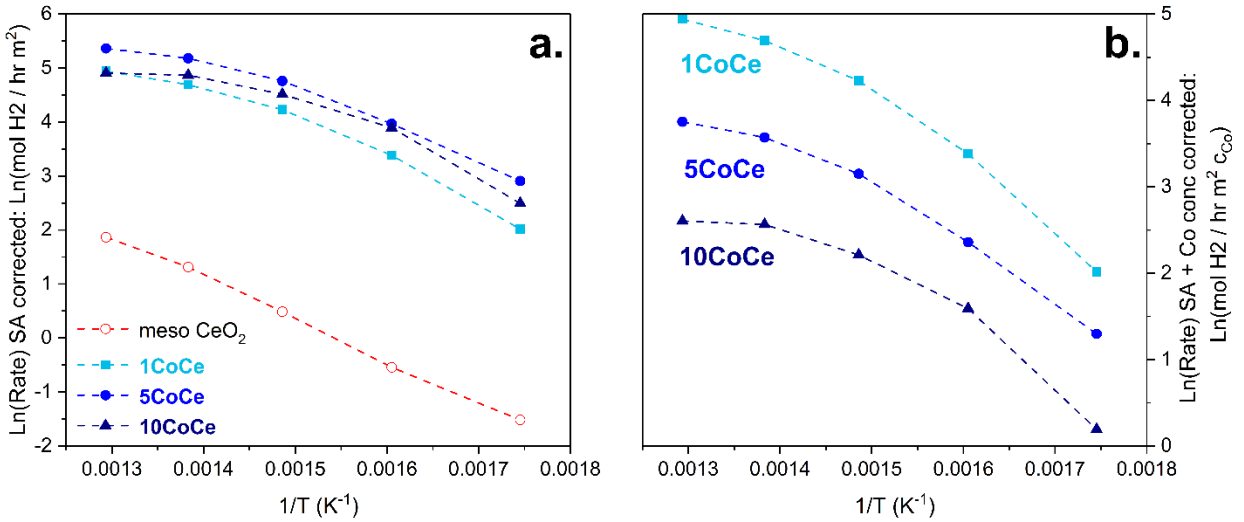

Figure 5: Activity plots for WGS catalytic activity over mesoporous catalysts normalized by surface area (a) and by surface area in addition to cobalt loading (b). Temperatures range from 500°C (1/T = 0.0013 K^{-1}) to 300°C (1/T = 0.0017 K^{-1}) in 50°C increments.

The mesoporous Co/CeO_2 catalysts were evaluated for their activity for the high temperature WGS reaction. The cobalt containing catalysts were found to exhibit greater activity than the bare mesoporous CeO_2 material[24] by approximately 3 orders of magnitude when normalized by surface area (Figure 5a). This significant increase suggests that catalytic pathways involving cobalt are predominantly responsible for catalytic activity in these materials. Since the cobalt is likely highly dispersed with no evidence of phase segregation, activity was further normalized by the total nominal cobalt content (Figure 5b). The activity per unit cobalt was observed to decrease with increasing cobalt concentration. Furthermore, a significant deviation from linearity at higher temperatures was observed to intensify as cobalt content was increased and is most obvious for **10CoCe**. This deviation suggests catalyst deactivation at higher temperatures that is likely related to total cobalt content.

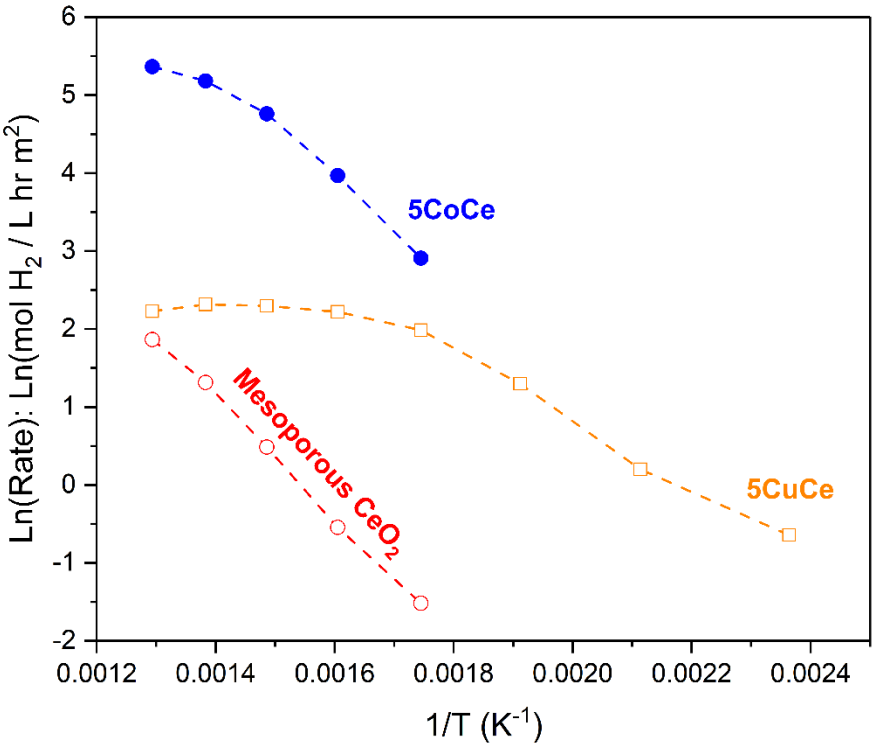

Figure 6: Activity plots for WGS catalytic activity over mesoporous copper and cobalt catalysts, normalized to surface area. Temperatures range from 500°C (1/T = 0.0013 K-1) to 150°C (1/T = 0.00236 K-1) in 50°C increments.

The WGS activity of **5CoCe** was also compared to a similarly prepared mesoporous 5% Cu/CeO_2 catalyst (**5CuCe**) that has been previously evaluated for its low temperature WGS activity[25] (Figure 6). This comparison provides evidence for the superiority of the cobalt loaded catalyst over copper at temperatures above approximately 300°C.

Active bulk Structure

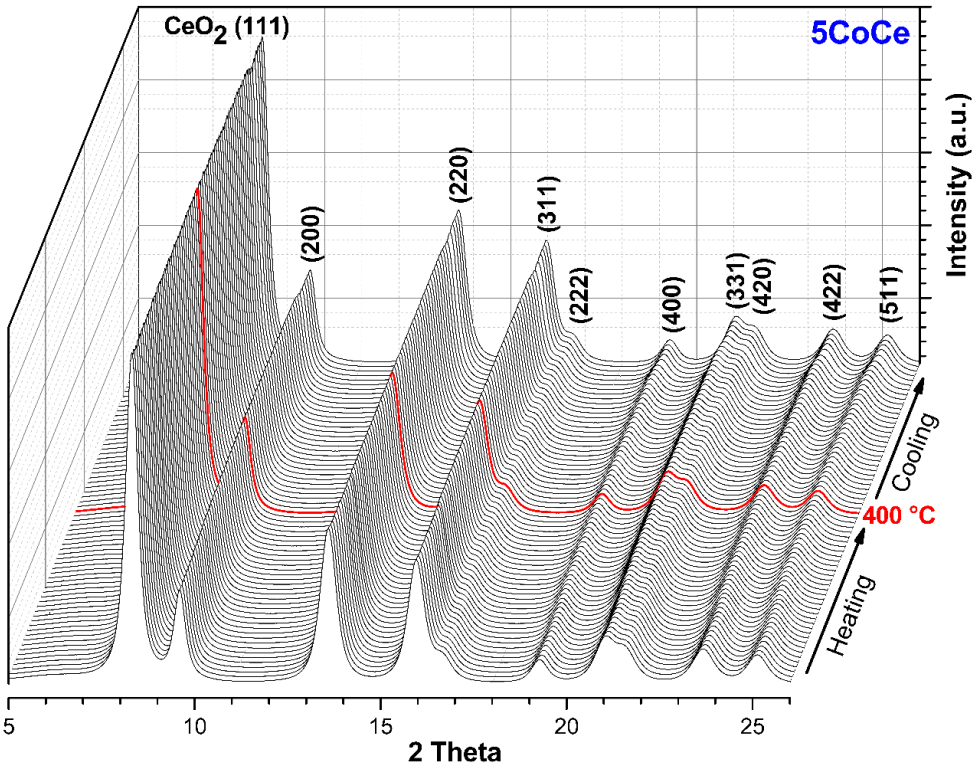

*Figure 7: Operando X-ray diffraction patterns of **5CoCe** under WGS reaction conditions*

Operando synchrotron X-ray diffraction (XRD) was utilized in order to study the changes in the bulk crystalline structure of the mesoporous Co/CeO_2 catalysts as they were heated stepwise under WGS reactant gas flow (5% CO, 3% H_2O, balance He). Powder XRD patterns of **5CoCe** collected under these conditions are presented in Figure 7. Similar waterfall plots were prepared for **1CoCe** (Figure S4) and **10CoCe** (Figure S5) as well.

The CeO_2 fluorite type lattice was the sole crystalline phase observed over the course of all operando XRD experiments. The absence of any segregated cobalt oxide or metal phase suggests that the Co/CeO_2 solid solution is robust under reaction conditions, although diffraction measurements do not rule out the presence of small segregated cobalt clusters with sizes below the diffraction limit or segregation of an amorphous phase.

The Rietveld method[32] was used to fit a model CeO_2 fluorite structure to each diffraction pattern. Using this refinement method, the average crystallite size was determined to be 6.2 nm for **1CoCe**, 6.8 nm for **5CoCe** and 6.0 nm for **10CoCe**, which are slightly larger values than those determined by TEM. This sort of discrepancy is common since TEM is a highly localized technique, whereas XRD measurements represent an ensemble average of all exposed crystallites. The CeO_2 crystallite size remains stable without aggregation under reaction conditions.

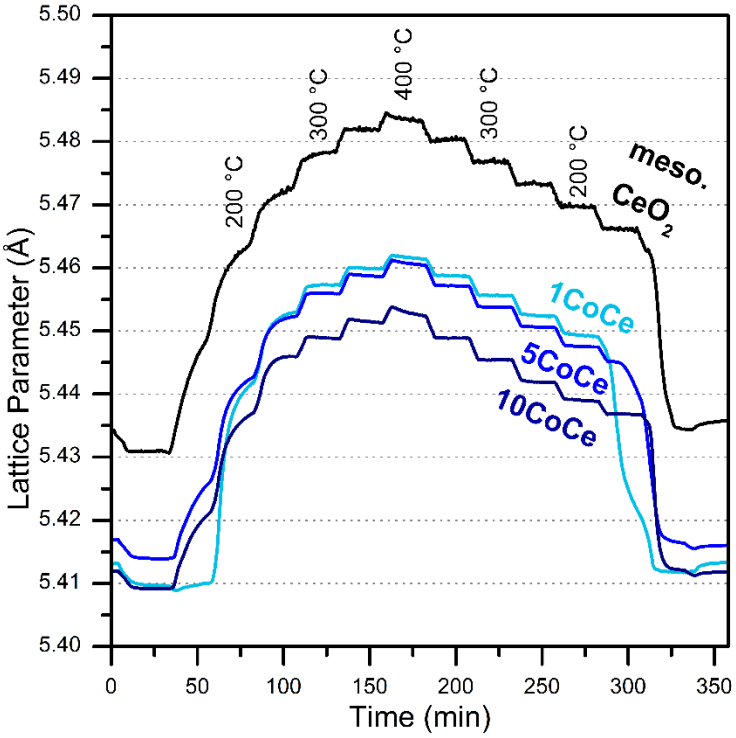

Figure 8: CeO_2 lattice parameters from Rietveld refinement of models fitted to operando XRD data.

The CeO_2 lattice parameters of bare mesoporous CeO_2, as well as mesoporous Co/CeO_2 catalysts over the course of the operando XRD experiments are plotted in Figure 8. The absolute lattice parameter of cobalt containing samples was observed to be significantly smaller than that

of pure mesoporous CeO_2 at all temperatures, which may be attributed to the substitution of Ce^{4+} (r = 0.97 Å) with Co^{2+} (r = 0.65 Å) in the fluorite lattice[44].

Upon heating the materials to 100 °C, a small contraction in the lattice was observed, likely related to the removal of precursor materials. Significant lattice expansion was observed for all samples upon heating between 100 °C and 250 °C. The cause for this expansion is most likely the reduction of Ce^{4+} (r = 0.97 Å) to Ce^{3+} (r = 1.14 Å) and formation of oxygen vacancies in the bulk of the CeO_2 material[45-46]. The shallow stepwise lattice expansion pattern visible at temperatures above approximately 250 °C is largely linear with temperature and is consistent with thermal expansion of cerium oxide[47]. This observation indicates that the majority of bulk cerium reduction takes place at temperatures under 300 °C, which contrasts with the increase in surface Ce^{3+} concentration until 400 °C observed during ambient pressure XPS measurements (Figure 4). The discrepancy suggests that the exposed surfaces of the catalyst materials are more readily reducible than the bulk under WGS reaction conditions. The reduced state of the CeO_2 bulk was maintained as the catalysts were cooled to 200 - 150 °C under reaction conditions, after which a rapid lattice contraction was observed, indicating re-oxidation of the oxide to its pre-reaction state.

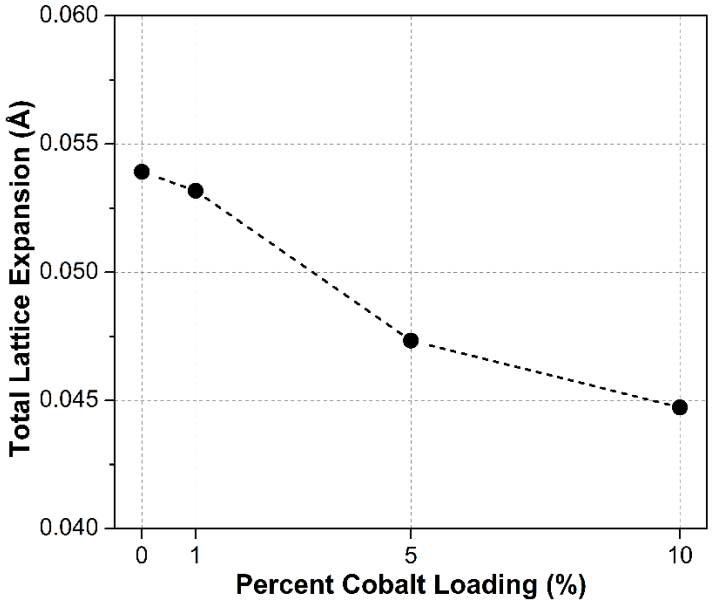

Figure 9: Total CeO_2 lattice expansion during operando XRD experiments

Relative bulk reducibility of catalyst materials was observed to vary with cobalt loading. In order to evaluate this reducibility factor, the minimum lattice parameter was subtracted from the maximum lattice parameter after the refinement analysis of each operando XRD experiment. The resulting total lattice expansion was plotted against cobalt concentration in Figure 9. Since the thermal expansion component for each sample is nearly constant and significantly smaller than the component of lattice expansion due to cerium reduction, the total lattice expansion is analogous to the relative extent of bulk CeO_2 reducibility under WGS conditions. Using this metric, the introduction of cobalt into the mesoporous CeO_2 was observed to inhibit the reduction of cerium. Since cerium reduction is associated with the formation of catalytically important oxygen vacancy sites, increasing cobalt concentration likely creates an adverse effect on activity.

Cobalt Chemical State

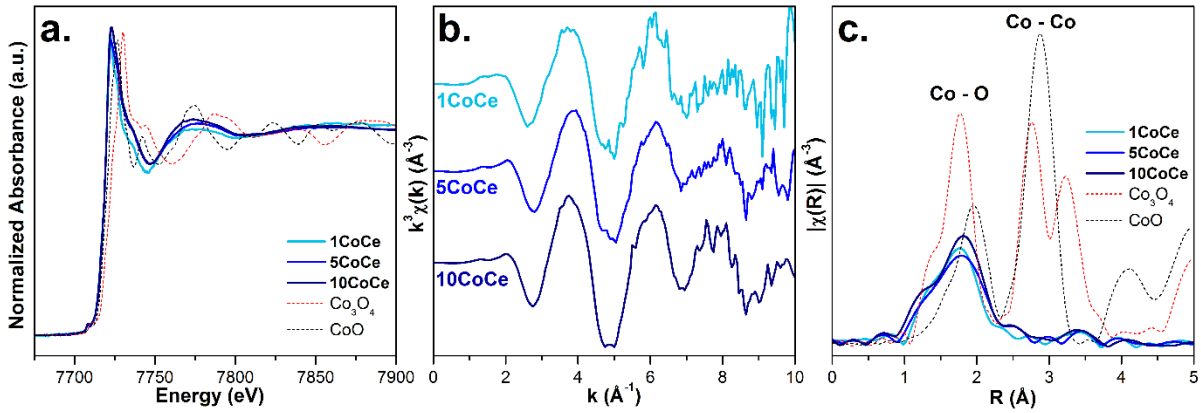

Figure 10: Co K-edge EXAFS results for mesoporous Co/CeO_2 materials: (a) Energy, (b) k-space, and (c) radial distribution function plots.

Cobalt K-edge X-ray absorption measurements were conducted in order to elucidate the state and behavior of the cobalt content in the mesoporous Co/CeO_2 materials. Analysis of EXAFS data collected for fresh samples (Figure 10) suggests that cobalt exists in an oxidized state, as evidenced by the short distance Co – O feature visible in the radial distribution function plot. The feature at approximately 1.8 Å is roughly consistent with the Co – O peak measured for Co_3O_4 and slightly below the Co – O peak measured for CoO. All features after approximately 2.5 Å are of very low intensity. Notably, the absence of any Co – Co features[48] rules out the presence of segregated cobalt oxide (or cobalt metal) phase in the fresh mesoporous Co/CeO_2 materials.

An examination of the state of cobalt under reaction conditions was carried out by measuring Co K-edge XANES while flowing WGS reactant gases (5% CO, 3% H_2O, balance He) and heating the samples. The resulting operando XANES spectra are documented in Figure 11. Since the cobalt content in mesoporous Co/CeO_2 samples does not exist as any segregated oxide phase, the line shapes of the absorption spectra may not be attributed to a linear combination of oxide or metal standards. Nevertheless, metallic cobalt and CoO standards were

included as reference materials for these measurements. Reliable EXAFS data was not obtained for samples under operando conditions due to limitations associated with X-ray absorption by the quartz capillary as well as the highly absorbing cerium oxide content of the samples.

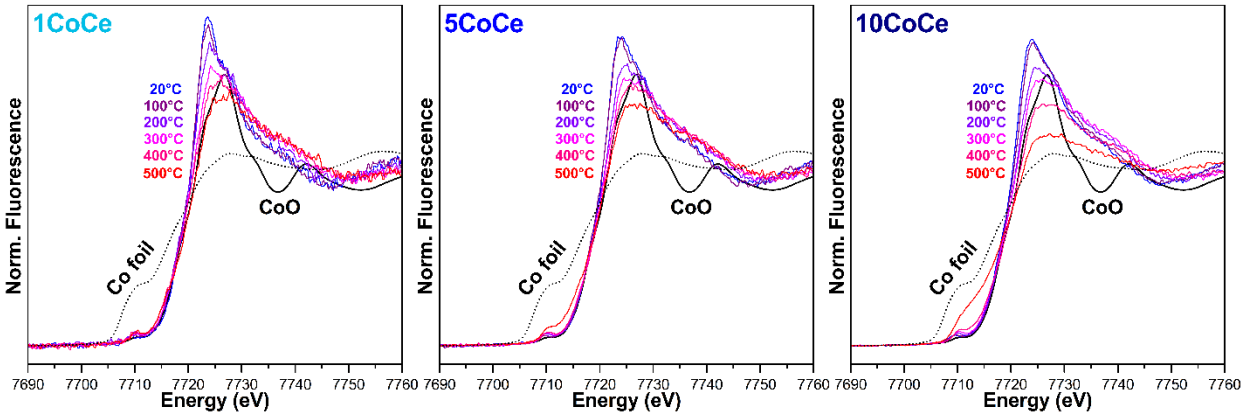

Figure 11: Operando Co K-edge XANES of mesoporous Co/CeO_2 materials under water-gas shift reaction conditions.

The notable components of the operando XANES spectra include the position of the edge, the position of the white line, the intensity of the white line, and the nature of the pre-edge feature. Regardless of cobalt concentration, the room temperature intensity and position of the white line is indicative of an oxidized cobalt species. With increasing temperature, the intensity of the white line decreases and its position shifts to higher energy, a phenomenon typically associated with cobalt reduction. The extent of this change with temperature, however, differs with concentration. In **10CoCe**, the white line intensity is decreased significantly more at higher temperatures than that of **5CoCe or 1CoCe**.

A small pre-edge feature around 7710 eV is visible in the room temperature XANES for all samples. In **1CoCe**, this feature remains approximately constant at all temperatures. In **5CoCe**, a change in the shape of this region is visible at 500 °C, when the pre-edge feature is observed to increase in intensity. This change is accompanied by a lower energy rise of the Co K

edge. In **10CoCe**, this behavior is significantly more apparent. The increase in the pre-edge feature intensity and accompanying edge shift are observed at 400 °C, and intensify as the sample is further heated to 500 °C. This pre-edge behavior is typically associated with the reduction of cobalt species to a metallic Co^0 state[49].

Operando XANES results suggest that the cobalt content is reduced with increasing temperature under WGS reactant conditions. Increasing concentration of cobalt in the sample is associated with a greater degree of cobalt reduction. Small metallic clusters may have been formed at 400-500 °C, particularly in the **10CoCe** sample. The size of these clusters would need to be below the diffraction limit, however, as no metallic cobalt phase was observed during operando X-ray diffraction experiments. Furthermore, the high-temperature changes in the state of cobalt in **10CoCe** (and to a lesser extent, **5CoCe**) may help explain the non-linearity in the activity measurements at 400-500 °C (Figure 5). In correlation with XANES observations, the non-linearity or downturn in activity is most obvious in **10CoCe**, but is also present in **5CoCe** as well. A negative causal relationship between the formation of small Co^0 metal clusters and catalytic activity would suggest that the active cobalt species is oxidized cobalt within the cerium oxide fluorite lattice. The CeO_2 lattice likely serves to stabilize cobalt in an oxidized state through favorable metal support interactions, allowing this active species to exist in the highly reducing WGS reaction environment.

Operando Surface Chemistry

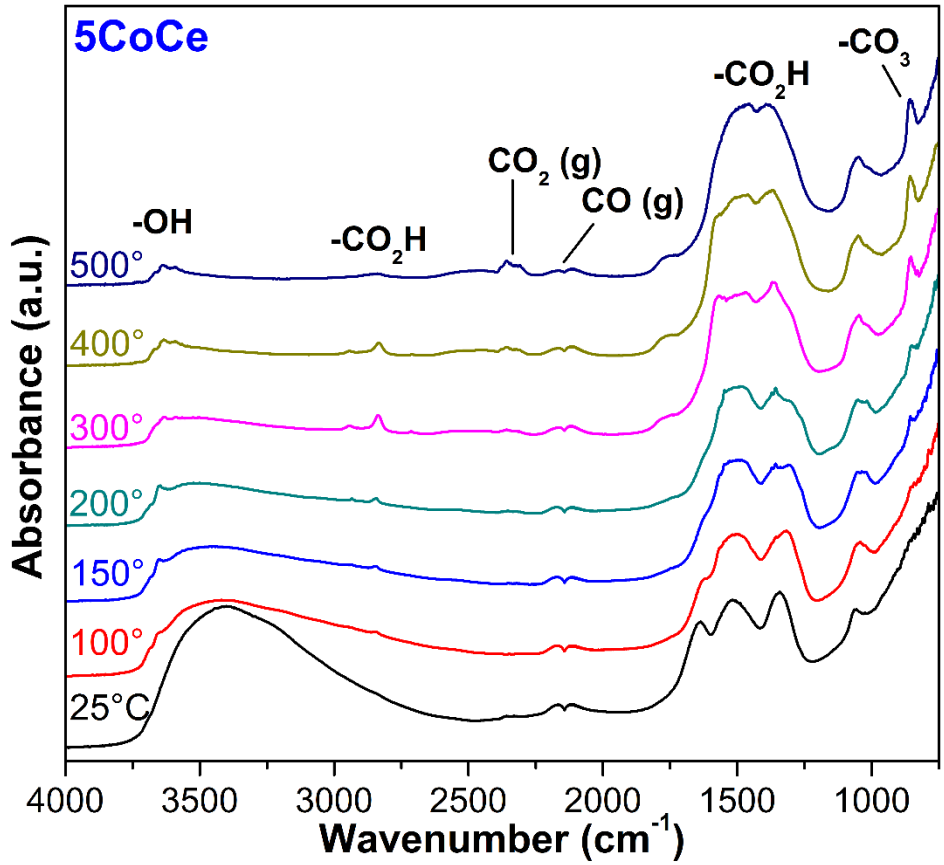

*Figure 12: DRIFTS of **5CoCe** under WGS reaction conditions*

Operando infrared spectroscopy (DRIFTS) was used to examine chemical species present on the surface of the mesoporous Co/CeO_2 catalysts under WGS reaction conditions. Representative DRIFTS spectra collected for **5CoCe** are plotted in Figure 12. Similar plots were prepared for **1CoCe** (Figure S6) and **10CoCe** (Figure S7). At room temperature, a broad feature around 3300 cm^{-1} indicates the presence of water, and another feature at 1635 cm^{-1} corresponds to water that has been molecularly adsorbed onto the catalyst surface[50]. As the temperature is increased, these features are removed and are replaced with smaller peaks around 3600 cm^{-1} that correspond to hydroxyl species on cerium oxide[51-52]. These hydroxyl species are formed following the dissociation of H_2O as a part of the WGS reaction. Around 150 °C, the development of several peaks between 3000 cm^{-1} and 2500 cm^{-1} is evident. The three peaks at

2932, 2842, and 2721 cm^{-1} correspond to δ(C-H) + ν_s(OCO), ν(C-H), and 2δ(C-H) of bidentate formate on CeO_2, respectively[51, 53]. Additional formate peaks are present in the region between 1750 and 1250 cm^{-1}, but this area is difficult to deconvolute. A feature at around 855 cm^{-1} also develops around 150 °C, which may correspond to various configurations of carbonate species on the CeO_2 surface[53].

As the temperature is increased to the catalytically active conditions between 300 and 500 °C, a gas phase CO_2 feature is evident, indicating WGS catalytic activity. Furthermore, the bidentate formate features decrease in intensity as this species becomes labile on the catalyst surface. The carbonate feature continues to increase with temperature, however. This behavior was documented on bare mesoporous CeO_2 as well[24], and may be attributed to the affinity of CeO_2 (100) surfaces for strongly binding tridentate carbonate[54].

A comparison of DRIFTS spectra for the studied catalyst materials at 400 °C is presented in Figure 13. The intensity of features associated with surface hydroxyl species is observed to decrease as cobalt concentration increases. This observation corroborates our operando X-ray diffraction experiments, which suggest a decrease in oxygen vacancy sites (H_2O splitting sites) with increasing cobalt concentration (Figure 9). The intensity of bands associated with bidentate formate also decreases with increasing cobalt concentration. Formate species have been previously identified as a potential intermediates[24] in the associative pathway[22] for the WGS reaction over bare mesoporous CeO_2. This pathway accounts for a greater portion of catalytic activity over catalysts with smaller cobalt loading.

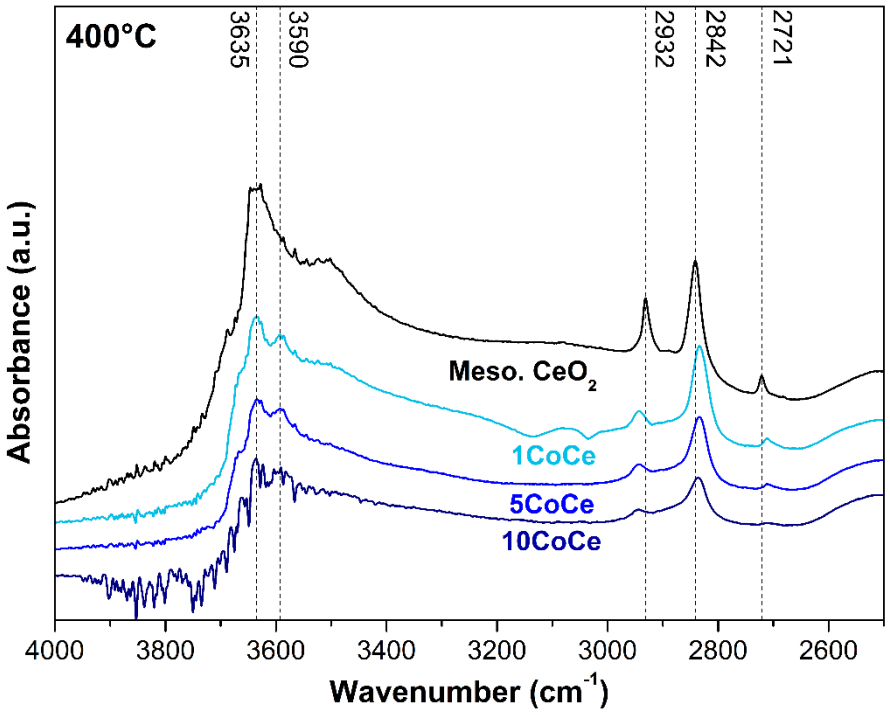

Figure 13:DRIFTS of catalyst materials under WGS reaction conditions at 400 °C

Conclusion

Following the development of a novel and catalytically active mesoporous morphology of cerium oxide, we have synthesized, tested, and characterized mesoporous Co/CeO_2 catalysts with varying cobalt concentrations (**1CoCe**, **5CoCe**, and **10CoCe**). Morphological examination of the material revealed a mesoporous structure consisting of highly crystalline and monodisperse nanoparticles with a fluorite type structure similar to CeO_2. Cobalt was observed by EDX to be present in concentrations in agreement with nominal loadings and well dispersed within the materials. Imaging, scattering and spectroscopic techniques did not reveal evidence of any segregated cobalt or cobalt oxide phase, suggesting that cobalt exists primarily in a solid solution state within the ceria lattice.

The mesoporous Co/CeO_2 catalysts were found to be active for water-gas shift reaction in the 300-500 °C temperature range. When normalized by cobalt content, the lowest loading (**1CoCe**) exhibited greatest activity per unit cobalt. Under reaction conditions, reduction of surface and bulk cerium was observed, as well as partial reduction of the cobalt content. Catalysts with higher cobalt loadings (**5CoCe** and to a greater extent **10CoCe**) were found to exhibit deactivation behavior at temperatures above 400 °C, possibly related to the segregation of very small clusters of metallic cobalt. Operando XRD and DRIFTS experiments suggest a more facile formation of active oxygen vacancy sites on catalysts with lower cobalt loadings, particularly **1CoCe**, providing a likely explanation for enhanced activity. Additional associative pathways may also be present, as evidenced by the DRIFTS observations of carbonaceous surface species under WGS reaction conditions.

The reaction environment characterization of these low cobalt loading catalysts is a part of an ongoing effort to foster an understanding of the structural, chemical, and mechanistic properties of catalytic materials for industrially important reactions like the water-gas shift. These insights may aid in the development of new and inexpensive catalysts through evidence based material design and synthesis.

Supporting Information Description

The supporting information for this work consists of 7 figures referred to throughout this text as Figures S1 through S7. Figures consist of additional microscopy, X-ray diffraction, and infrared spectroscopy data.

Acknowledgements

The research carried out at Brookhaven National Laboratory was supported by the U.S. Department of Energy, Office of Science and Office of Basic Energy Sciences under contract No. DE-SC0012704. This research used resources of the 8-ID (ISS) beamline of the National Synchrotron Light Source II, a U.S. Department of Energy (DOE) Office of Science User Facility operated for the DOE Office of Science by Brookhaven National Laboratory under Contract No. DE-SC0012704. This work also used resources of the Advanced Photon Source (17B-M), a U.S. Department of Energy (DOE) Office of Science User Facility operated for the DOE Office of Science by Argonne National Laboratory under Contract No. DE-AC02-06CH11357. J. L. is a Serra Hunter Fellow and is grateful to the ICREA Academia Program and MINECO/FEDER grant ENE2015-63969-R. SLS acknowledges support from the U.S. Department of Energy, Office of Basic Energy Sciences, Division of Chemical, Biological and Geological Sciences (grant DE-FG02-86ER13622A00), as well as the assistance of the Bioscience Electron Microscopy Laboratory of the University of Connecticut and grant # 1126100 for the purchase of the FEI NovaSEM. The authors also acknowledge Dr. Taejin Kim and Mr. Xiaojun Chan from Stony Brook University for making available their infrared spectroscopy facilities for the purposes of this work.

Table of Contents (TOC) Image

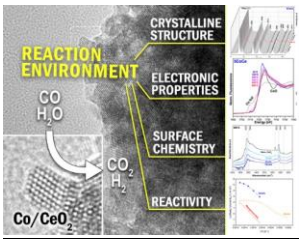

References

1. Dincer, I.; Acar, C., Review and Evaluation of Hydrogen Production Methods for Better Sustainability. *International Journal of Hydrogen Energy* **2015**, *40*, 11094-11111.
2. Hickman, D. A.; Schmidt, L. D., Production of Syngas by Direct Catalytic Oxidation of Methane. *Science* **1993**, *259*, 343-346.
3. Li, Q.; He, R.; Gao, J.-A.; Jensen, J. O.; Bjerrum, N. J., The Co Poisoning Effect in Pemfcs Operational at Temperatures up to 200°C. *Journal of The Electrochemical Society* **2003**, *150*, A1599-A1605.
4. Newsome, D. S., The Water-Gas Shift Reaction. *Catalysis Reviews* **1980**, *21*, 275-318.
5. Batista, M. S.; Santiago, E. I.; Assaf, E. M.; Ticianelli, E. A., Evaluation of the Water-Gas Shift and Co Methanation Processes for Purification of Reformate Gases and the Coupling to a Pem Fuel Cell System. *Journal of Power Sources* **2005**, *145*, 50-54.
6. Kolb, G.; Schurer, J.; Tiemann, D.; Wichert, M.; Zapf, R.; Hessel, V.; Lowe, H., Fuel Processing in Integrated Micro-Structured Heat-Exchanger Reactors. *Journal of Power Sources* **2007**, *171*, 198-204.
7. Spivey, J. J., Catalysis in the Development of Clean Energy Technologies. *Catalysis Today* **2005**, *100*, 171-180.
8. Sun, Y.; Hla, S. S.; Duffy, G. J.; Cousins, A. J.; French, D.; Morpeth, L. D.; Edwards, J. H.; Roberts, D. G., Effect of Ce on the Structural Features and Catalytic Properties of La(0.9−X)Cexfeo3 Perovskite-Like Catalysts for the High Temperature Water–Gas Shift Reaction. *International Journal of Hydrogen Energy* **2011**, *36*, 79-86.
9. Keiski, R. L.; Salmi, T.; Niemistö, P.; Ainassaari, J.; Pohjola, V. J., Stationary and Transient Kinetics of the High Temperature Water-Gas Shift Reaction. *Applied Catalysis A: General* **1996**, *137*, 349-370.
10. Salmi, T.; Boström, S.; Lindfors, L. E., A Dynamic Study of the Water-Gas Shift Reaction over an Industrial Ferrochrome Catalyst. *Journal of Catalysis* **1988**, *112*, 345-356.
11. Zhu, M.; Wachs, I. E., Iron-Based Catalysts for the High-Temperature Water–Gas Shift (Ht-Wgs) Reaction: A Review. *ACS Catalysis* **2016**, *6*, 722-732.
12. Meshkani, F.; Rezaei, M., High Temperature Water Gas Shift Reaction over Promoted Iron Based Catalysts Prepared by Pyrolysis Method. *International Journal of Hydrogen Energy* **2014**, *39*, 16318-16328.
13. Fu, Q.; Saltsburg, H.; Flytzani-Stephanopoulos, M., Active Nonmetallic Au and Pt Species on Ceria-Based Water-Gas Shift Catalysts. *Science* **2003**, *301*, 935-938.
14. Hilaire, S.; Wang, X.; Luo, T.; Gorte, R. J.; Wagner, J., A Comparative Study of Water-Gas-Shift Reaction over Ceria Supported Metallic Catalysts. *Applied Catalysis A: General* **2001**, *215*, 271-278.
15. Li, Y.; Fu, Q.; Flytzani-Stephanopoulos, M., Low-Temperature Water-Gas Shift Reaction over Cu- and Ni-Loaded Cerium Oxide Catalysts. *Applied Catalysis B: Environmental* **2000**, *27*, 179-191.
16. Si, R.; Flytzani-Stephanopoulos, M., Shape and Crystal-Plane Effects of Nanoscale Ceria on the Activity of Au-Ceo2 Catalysts for the Water–Gas Shift Reaction. *Angewandte Chemie International Edition* **2008**, *47*, 2884-2887.
17. Chueh, W. C.; Falter, C.; Abbott, M.; Scipio, D.; Furler, P.; Haile, S. M.; Steinfeld, A., High-Flux Solar-Driven Thermochemical Dissociation of Co2 and H2o Using Nonstoichiometric Ceria. *Science* **2010**, *330*, 1797-1801.
18. Mullins, D. R., The Surface Chemistry of Cerium Oxide. *Surface Science Reports* **2015**, *70*, 42-85.
19. Farmer, J. A.; Campbell, C. T., Ceria Maintains Smaller Metal Catalyst Particles by Strong Metal-Support Bonding. *Science* **2010**, *329*, 933-936.
20. Hansen, H. A.; Wolverton, C., Kinetics and Thermodynamics of H2o Dissociation on Reduced Ceo2(111). *The Journal of Physical Chemistry C* **2014**, *118*, 27402-27414.

21. Putna, E. S.; Vohs, J. M.; Gorte, R. J., Evidence for Weakly Bound Oxygen on Ceria Films. *The Journal of Physical Chemistry* **1996**, *100*, 17862-17865.
22. Rodriguez, J. A.; Liu, P.; Hrbek, J.; Evans, J.; Pérez, M., Water Gas Shift Reaction on Cu and Au Nanoparticles Supported on Ceo2(111) and Zno(000-1): Intrinsic Activity and Importance of Support Interactions. *Angewandte Chemie International Edition* **2007**, *46*, 1329-1332.
23. Poyraz, A. S.; Kuo, C.-H.; Biswas, S.; King'ondu, C. K.; Suib, S. L., A General Approach to Crystalline and Monomodal Pore Size Mesoporous Materials. *Nat Commun* **2013**, *4*.
24. Guild, C. J., et al., Water-Gas-Shift over Metal-Free Nanocrystalline Ceria: An Experimental and Theoretical Study. *ChemCatChem* **2017**, *9*, 1373-1377.
25. Vovchok, D., et al., Cu Supported on Mesoporous Ceria: Water Gas Shift Activity at Low Cu Loadings through Metal-Support Interactions. *Physical Chemistry Chemical Physics* **2017**.
26. Jha, A.; Jeong, D.-W.; Lee, Y.-L.; Nah, I. W.; Roh, H.-S., Enhancing the Catalytic Performance of Cobalt Oxide by Doping on Ceria in the High Temperature Water-Gas Shift Reaction. *RSC Advances* **2015**, *5*, 103023-103029.
27. Lee, Y.-L., et al., Optimization of Cobalt Loading in Co–Ceo2 Catalyst for the High Temperature Water–Gas Shift Reaction. *Topics in Catalysis* **2017**, *60*, 721-726.
28. Xie, X.; Li, Y.; Liu, Z.-Q.; Haruta, M.; Shen, W., Low-Temperature Oxidation of Co Catalysed by Co3o4 Nanorods. *Nature* **2009**, *458*, 746.
29. Fairley, N.; Ltd, C. S., *Casaxps Manual 2.3.15: Casaxpx Processing Software for Xps Spectra*; Casa Software Limited, 2009.
30. Chupas, P. J.; Chapman, K. W.; Kurtz, C.; Hanson, J. C.; Lee, P. L.; Grey, C. P., A Versatile Sample-Environment Cell for Non-Ambient X-Ray Scattering Experiments. *Journal of Applied Crystallography* **2008**, *41*, 822-824.
31. Toby, B. H.; Von Dreele, R. B., Gsas-Ii: The Genesis of a Modern Open-Source All Purpose Crystallography Software Package. *Journal of Applied Crystallography* **2013**, *46*, 544-549.
32. Albinati, A.; Willis, B. T. M., The Rietveld Method in Neutron and X-Ray Powder Diffraction. *Journal of Applied Crystallography* **1982**, *15*, 361-374.
33. Ravel, B.; Newville, M., Athena, Artemis, Hephaestus: Data Analysis for X-Ray Absorption Spectroscopy Using Ifeffit. *J Synchrotron Radiat* **2005**, *12*, 537-41.
34. Deshpande, S.; Patil, S.; Kuchibhatla, S. V.; Seal, S., Size Dependency Variation in Lattice Parameter and Valency States in Nanocrystalline Cerium Oxide. *Applied Physics Letters* **2005**, *87*, 133113.
35. Brunauer, S.; Emmett, P. H.; Teller, E., Adsorption of Gases in Multimolecular Layers. *Journal of the American Chemical Society* **1938**, *60*, 309-319.
36. Istomin, S. Y., et al., An Unusual High-Spin Ground State of Co3+ in Octahedral Coordination in Brownmillerite-Type Cobalt Oxide. *Dalton Transactions* **2015**, *44*, 10708-10713.
37. Lin, H. J., et al., Local Orbital Occupation and Energy Levels of Co in Naxcoo2: A Soft X-Ray Absorption Study. *Physical Review B* **2010**, *81*, 115138.
38. Wang, J.; Zhou, J.; Hu, Y.; Regier, T., Chemical Interaction and Imaging of Single Co3o4/Graphene Sheets Studied by Scanning Transmission X-Ray Microscopy and X-Ray Absorption Spectroscopy. *Energy & Environmental Science* **2013**, *6*, 926-934.
39. Smythe, D. J.; Brenan, J. M.; Bennett, N. R.; Regier, T.; Henderson, G. S., Quantitative Determination of Cerium Oxidation States in Alkali-Aluminosilicate Glasses Using M4,5-Edge Xanes. *Journal of Non-Crystalline Solids* **2013**, *378*, 258-264.
40. Bêche, E.; Charvin, P.; Perarnau, D.; Abanades, S.; Flamant, G., Ce 3d Xps Investigation of Cerium Oxides and Mixed Cerium Oxide (Cextiyoz). *Surface and Interface Analysis* **2008**, *40*, 264-267.
41. Paparazzo, E., On the Curve-Fitting of Xps Ce(3d) Spectra of Cerium Oxides. *Materials Research Bulletin* **2011**, *46*, 323-326.

42. Chen, L.; Fleming, P.; Morris, V.; Holmes, J. D.; Morris, M. A., Size-Related Lattice Parameter Changes and Surface Defects in Ceria Nanocrystals. *The Journal of Physical Chemistry C* **2010**, *114*, 12909-12919.
43. Zhang, F.; Wang, P.; Koberstein, J.; Khalid, S.; Chan, S. W., Cerium Oxidation State in Ceria Nanoparticles Studied with X-Ray Photoelectron Spectroscopy and Absorption near Edge Spectroscopy. *Surface Science* **2004**, *563*, 74-82.
44. Ansari, A. A.; Labis, J.; Alam, M.; Ramay, S. M.; Ahmad, N.; Mahmood, A., Effect of Cobalt Doping on Structural, Optical and Redox Properties Cerium Oxide Nanoparticles. *Phase Transitions* **2016**, *89*, 261-272.
45. Xu, W. Q.; Si, R.; Senanayake, S. D.; Llorca, J.; Idriss, H.; Stacchiola, D.; Hanson, J. C.; Rodriguez, J. A., In Situ Studies of Ceo2-Supported Pt, Ru, and Pt-Ru Alloy Catalysts for the Water-Gas Shift Reaction: Active Phases and Reaction Intermediates. *Journal of Catalysis* **2012**, *291*, 117-126.
46. Wang, X.; Rodriguez, J. A.; Hanson, J. C.; Gamarra, D.; Martínez-Arias, A.; Fernández-García, M., In Situ Studies of the Active Sites for the Water Gas Shift Reaction over Cu−Ceo2 Catalysts: Complex Interaction between Metallic Copper and Oxygen Vacancies of Ceria. *The Journal of Physical Chemistry B* **2006**, *110*, 428-434.
47. Trovarelli, A., Catalytic Properties of Ceria and Ceo2-Containing Materials. *Catal Rev* **1996**, *38*, 439-520.
48. Rosen, J.; Hutchings, G. S.; Jiao, F., Synthesis, Structure, and Photocatalytic Properties of Ordered Mesoporous Metal-Doped Co3o4. *Journal of Catalysis* **2014**, *310*, 2-9.
49. Jacobs, G.; Williams, L.; Graham, U.; Sparks, D.; Davis, B. H., Low-Temperature Water-Gas Shift: In-Situ Drifts−Reaction Study of a Pt/Ceo2 Catalyst for Fuel Cell Reformer Applications. *The Journal of Physical Chemistry B* **2003**, *107*, 10398-10404.
50. Zhao, F., et al., Water-Gas Shift Reaction on Ni–W–Ce Catalysts: Catalytic Activity and Structural Characterization. *The Journal of Physical Chemistry C* **2014**, *118*, 2528-2538.
51. Binet, C.; Daturi, M.; Lavalley, J. C., Ir Study of Polycrystalline Ceria Properties in Oxidised and Reduced States. *Catalysis Today* **1999**, *50*, 207-225.
52. Yao, S. Y.; Xu, W. Q.; Johnston-Peck, A. C.; Zhao, F. Z.; Liu, Z. Y.; Luo, S.; Senanayake, S. D.; Martinez-Arias, A.; Liu, W. J.; Rodriguez, J. A., Morphological Effects of the Nanostructured Ceria Support on the Activity and Stability of Cuo/Ceo2 Catalysts for the Water-Gas Shift Reaction. *Phys Chem Chem Phys* **2014**, *16*, 17183-95.
53. Vayssilov, G. N.; Mihaylov, M.; Petkov, P. S.; Hadjiivanov, K. I.; Neyman, K. M., Reassignment of the Vibrational Spectra of Carbonates, Formates, and Related Surface Species on Ceria: A Combined Density Functional and Infrared Spectroscopy Investigation. *The Journal of Physical Chemistry C* **2011**, *115*, 23435-23454.
54. Albrecht, P. M.; Jiang, D.-e.; Mullins, D. R., Co2 Adsorption as a Flat-Lying, Tridentate Carbonate on Ceo2(100). *The Journal of Physical Chemistry C* **2014**, *118*, 9042-9050.